Pramana – J. Phys. (2019) 92:55
https://doi.org/10.1007/s12043-018-1711-1

© Indian Academy of Sciences

Comparative study of discharge characteristics and associated film growth for post-cathode and inverted cylindrical magnetron sputtering

R RANE[1,2,*], A JOSHI[3], S AKKIREDDY[1,2] and S MUKHERJEE[1,2]

[1]Institute for Plasma Research, Gandhinagar, Bhat, Ahmedabad 382 428, India
[2]Homi Bhabha National Institute, Anushakti Nagar, Mumbai 400 094, India
[3]LDRP College, Gandhinagar 382 015, India
*Corresponding author. E-mail: ramu@ipr.res.in

MS received 27 February 2018; revised 9 August 2018; accepted 29 August 2018;
published online 15 February 2019

Abstract. In this study, an experimental investigation of a DC cylindrical magnetron discharge for argon gas in post-cathode (i.e. direct) and hollow-cathode (i.e. inverted) configurations was carried out. The discharge properties at different externally applied magnetic fields and operating pressures were measured and compared for both the configurations. The discharge current (I)–voltage (V) characteristics obey $I \propto V^n$, where the value of n is in the range of 3–8. The discharge current increases linearly with the magnetic field in the post-cathode configuration, whereas it saturates at higher magnetic fields in the case of inverted configuration. Measurement of plasma potential indicated a considerable anode fall in the inverted magnetron configuration, whereas a negligible anode fall and strong cathode fall were observed in the case of post-cathode configuration. The plasma density and electron temperature, measured using a double Langmuir probe, were observed to be higher in the inverted magnetron configuration. The plasma density was found to be maximum at around 3–4 cm away from the respective inner electrode in both the configurations. A clear change in surface morphology of copper thin film was observed in the case of inverted magnetron configuration, which might be due to the extra ionisation near the anode owing to the anode fall.

Keywords. Cylindrical magnetron; magnetic field; thin film; plasma potential.

PACS Nos **52.25.–b; 52.25.Xz; 52.77.–j; 52.70.Ds**

1. Introduction

Magnetron sputtering sources are glow discharge plasmas in which magnetic fields are used in concert with the cathode surface to form electron traps which are so configured that the $\vec{E} \times \vec{B}$ electron-drift currents can close on themselves [1]. Magnetron discharge-based physical vapour deposition sources find applications in materials processing industry for the sputter deposition of thin films over a variety of components [2–4]. At typical operating pressure in these discharges, the electron mean free path is much greater than the Larmour radius and electrons can drift large distance in the $\vec{E} \times \vec{B}$ direction before they are scattered. However, the $\vec{E} \times \vec{B}$ drift current can be made to close on itself by using a suitable magnetic field geometry and cathode design resulting in effectively confining electrons within the discharge for longer periods. This leads to an increased ionisation efficiency and plasma density, thereby enabling the plasma generation at operating pressures lower than those required in similar unmagnetised devices. Ions from the plasma bombard the cathode – with energies comparable to the total potential difference across the electrodes – resulting in the emission of secondary electrons which eventually get accelerated in the cathode fall and improve ionisation further. The sputtering rates of the cathode are increased due to enhanced ion density and impact energies of the ions. At the same time, the transport of sputtered atoms improves due to lower operating pressures. Thus, the overall performance of the magnetron discharge is better than that of the unmagnetised discharge. There are many types of electrode designs and magnetic field configurations for magnetron sputtering discharge and the two most common configurations are: (i) planar magnetron and (ii) cylindrical magnetron

configurations. The DC sputtering discharge in coaxial metallic electrodes in the presence of magnetic field is called cylindrical magnetron [1,5]. There are two configurations of cylindrical magnetron, viz. post-cathode cylindrical magnetron and inverted or hollow cathode cylindrical magnetron. Cylindrical magnetron discharge is called post-cathode if the central electrode is the cathode and outer cylindrical chamber is the anode. In the swapped electrode arrangement, the discharge is called the inverted cylindrical magnetron discharge. The direction of the charged particle flux and surface area of the electrodes are the two prominent parameters that contribute to the differences in both the configurations. The cylindrical magnetron discharges can be used for thin film deposition on long cylindrical objects, complex-shaped substrates, etc. Because of its industrial applications, the cylindrical magnetron discharge has been studied experimentally and theoretically during the last few decades [1,5]. Generally, this study has been concentrated on the determination of various basic plasma parameters such as charged particle flux, their energy distribution, temperature, electric potential, etc. An extensive experimental and theoretical study of cylindrical magnetron discharge in post-cathode configuration has been reported by Van der Straaten *et al* [6,7]. The radial structure was investigated using the Monte–Carlo simulation technique and comparison was made with the fluid model [6]. The plasma parameters were measured using the cylindrical Langmuir probe [8]. The current–voltage characteristics of DC and radiofrequency (RF)-driven post-cathode cylindrical magnetron discharges were also studied [9]. Passoth *et al* [10] determined the plasma density by using a cylindrical Langmuir probe at different operating pressures and magnetic fields in a cylindrical magnetron discharge. The electrostatic instability in the presence of $\vec{E} \times \vec{B}$ flow in a DC cylindrical magnetron discharge plasma is also observed [11]. The substrate heating during the thin film deposition in post-cathode cylindrical magnetron sputtering sources was studied by Thornton [12]. The internal stresses in metallic films deposited by post-cathode cylindrical magnetron sputtering was also studied [13]. In summary, the post-cathode cylindrical magnetron is extensively studied by considering its application in thin film deposition. There are also a few reports on experimental study of inverted cylindrical magnetron discharge and its application. The transition from positive space charge to negative space charge is reported for an inverted cylindrical magnetron discharge [14]. The electrical and sputtering characteristics of 100 mm diameter inverted magnetron configuration were investigated in the past [15]. The calculations of electron distribution functions, radial distributions of the electron density, excitation and ionisation rates, and charged particle flux for both magnetron configurations were carried out by Golubovskii *et al* [16]. The electrical and optical characterisations of inverted magnetron in the pulsed mode have been performed [17]. The thin film deposition of titanium dioxide by DC hollow cathode magnetron sputtering is carried out in which the structural and surface properties of the films were studied [18]. Recently, calculation of heat absorbed by the substrate suspended inside the inverted cylindrical magnetron has been performed [19]. In the inverted configuration, surface area of the outer cathode is more compared to that of the central anode. The discharge characteristics of an inverted magnetron differ from the post-cathode configuration even though the principle of operation is the same [16]. Hence, understanding these differences can help in the technological application of these discharges in thin film deposition. In this work, we report a comparative study of post-cathode and inverted cylindrical magnetron discharges. The discharge current (I)–voltage (V) characteristics and discharge current (I)–magnetic field (B) characteristics were studied in both the configurations. The radial profile of plasma potential, electron temperature and plasma density was measured in both the configurations and compared. Finally, thin films of copper metal were deposited in both the configurations, characterised and compared.

2. Experimental set-up

The experimental set-up consists mainly of a vacuum compatible stainless steel (SS) chamber, target electrode, Helmholtz coil, pumping system, DC power supplies, etc. The SS chamber is of hollow cylindrical shape of 500 mm diameter and 800 mm length. This cylindrical chamber was placed in the horizontal position and acts as one of the two electrodes (outer electrode) necessary for plasma generation. An SS solid rod of 20 mm diameter and 400 mm length was placed in the middle of the vacuum chamber, along its horizontal axis. This rod-shaped electrode serves as an inner electrode. The schematic diagram of this cylindrical coaxial electrode configuration is shown in figure 1. The limiters are connected at both ends of the inner electrode to prevent the end losses of energetic electrons. In the post-cathode magnetron discharge, the inner electrode (steel rod) works as the cathode and the outer electrode (SS chamber) works as the anode. The discharge is known as inverted magnetron discharge if the electrode arrangement is swapped, i.e. the inner electrode works as the anode and the outer electrode works as the cathode. The schematic diagrams of these two configurations are also shown in figure 1. The distance between the

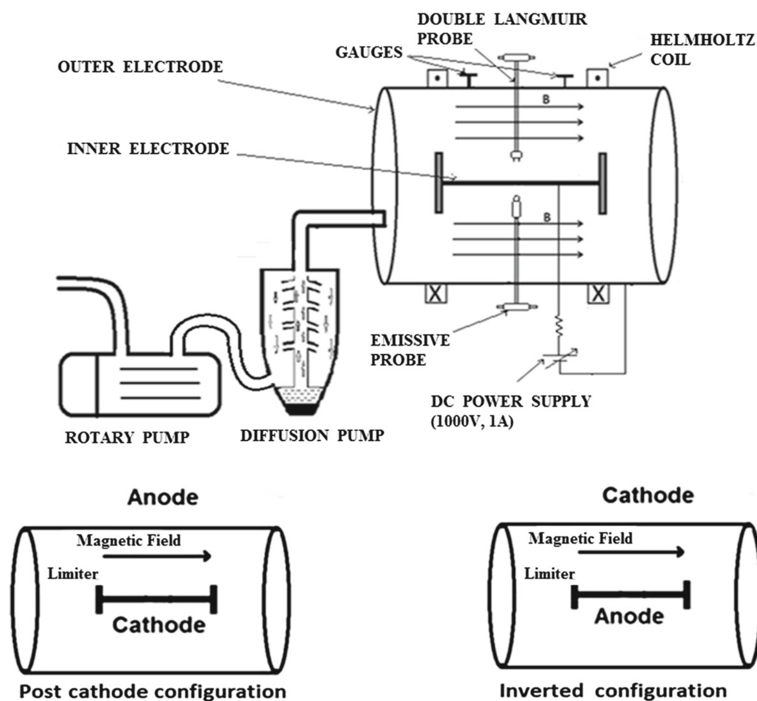

Figure 1. Schematic diagram of the experimental set-up.

inner electrode and the outer electrode was 240 mm. A Helmholtz coil was designed and constructed to obtain a uniform magnetic field inside the vacuum vessel, in the direction parallel to the longer axis of the central electrode. The magnetic field was mapped by measuring it at many points using a Hall probe and it was ensured that it is uniform in the entire volume between both the electrodes. The typical magnetic field profile in the axial and radial directions is shown in figure 2. A combination of rotary and diffusion pumps was used for obtaining the necessary base pressure which is of the order of 5×10^{-5} mbar. Argon (Ar) gas was used for the formation of plasma. In order to form the plasma, the pressure inside the vacuum vessel was increased from the base pressure to operating pressure which was varied within the range of 5×10^{-3}–5×10^{-2} mbar, by feeding argon gas using a gas dosing valve. A DC power supply (1000 V, 1 A) was used for biasing the electrodes, to form plasma in both the configurations. A current-limiting resistor was connected in series, in the line connecting the power supply to the electrode, which was also used for measuring the discharge current. The plasma potential was measured using an emissive probe. A 6 mm diameter loop, constructed out of 0.25 mm diameter tungsten wire of 15 mm length, was used as an emissive probe. The saturated floating potential measured with the emissive probe was considered as the plasma potential [20]. Electron temperature and plasma density were obtained from the *I*–*V* characteristics of a double

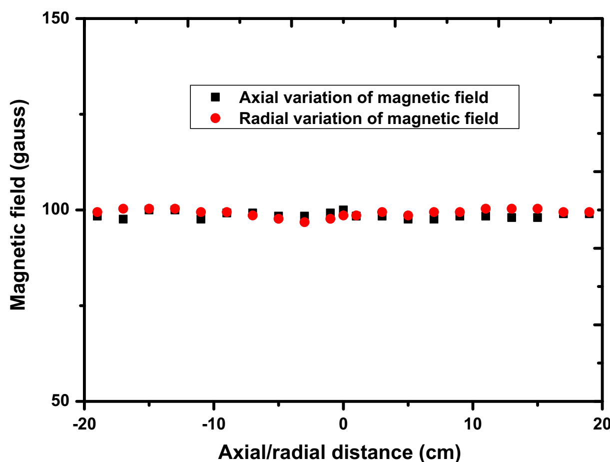

Figure 2. Magnetic field profile at 100 G. The axial profile is at zero radial position and radial profile is at zero axial position.

Langmuir probe. The double Langmuir probe was made from two single Langmuir probes of 0.25 mm diameter and 5 mm length, separated by 10 mm. The probe was placed inside the plasma such that it remains perpendicular to the magnetic field lines. Finally, copper thin film was deposited on silicon substrates in both the configurations. X-ray diffraction (XRD) and scanning electron microscopy (SEM) were used for studying the crystalline nature and surface morphology of the deposited films, respectively.

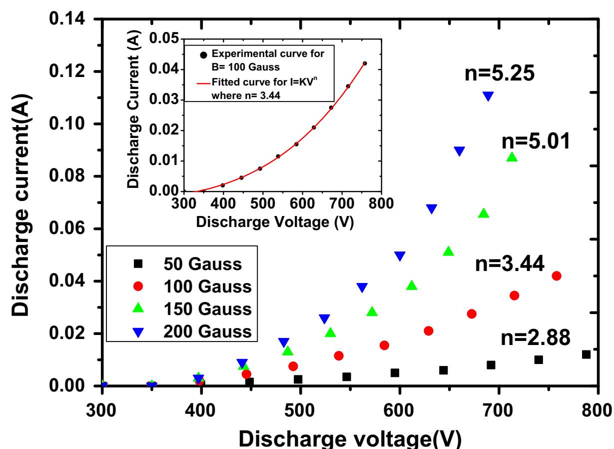

Figure 3. Current–voltage characteristics for the post-cathode.

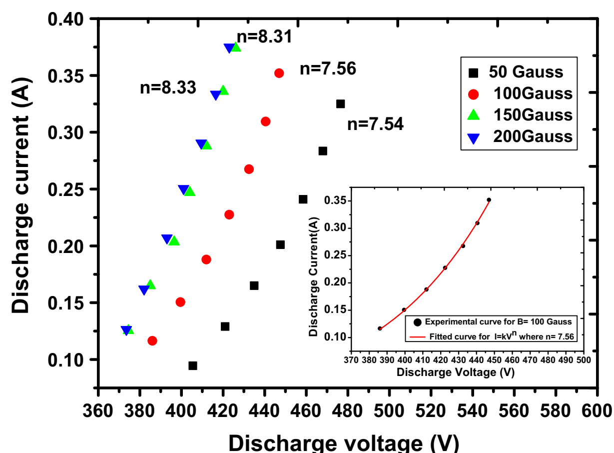

Figure 4. Current–voltage characteristics for the inverted magentron.

3. Results and discussion

3.1 *Current–voltage characteristics*

The current (I)–voltage (V) characteristics of the discharge, in both post-cathode and inverted magnetron configurations, were measured. The discharges were operated in the Ar environment at 5×10^{-3} mbar pressure, and at four different axial magnetic fields varying from 50 to 200 G. The I–V characteristics of the post-cathode and inverted magnetron configurations are shown in figures 3 and 4, respectively. In the post-cathode magnetron discharge, at a fixed magnetic field and operating pressure, the relation between the discharge current and the discharge voltage was found to be $I \propto V^n$, where n is in the range of 3–5. The inset graph of figure 3 shows the fitted I–V characteristic curve for a magnetic field of 100 G. Increasing the value of n with magnetic field shows more electron trapping in the discharge. Almost the same behaviour, of the form $I \propto V^n$, was observed at all four magnetic fields. A similar trend in the current–voltage curve was observed in the case of inverted magnetron discharge also. However, in this case, the value of n was found to be in the range of 7.5–8.5 (figure 4). The fitted I–V characteristics curve, in this case, for a magnetic field of 100 G is shown in the inset of figure 4. The value of n in an inverted magnetron discharge is clearly larger than that of the post-cathode magnetron discharge. In the inverted magnetron discharge, the electrons are confined by externally applied magnetic field, and hence the rate of electron loss by radial diffusion is reduced. Further, the secondary electron emission is also very high in the case of inverted magnetron discharge due to larger surface area of the cathode. That is why the value of exponent n is observed to be higher in the case of inverted magnetron discharge indicating higher efficiency of electron confinement in magnetron [1]. Accordingly, the absolute value of discharge current was observed to be higher in inverted magnetron discharge when compared to that in the post-cathode magnetron discharge under the same experimental conditions. The surface area of the cathode – which contributes to the secondary electron emission – is very much larger in the inverted magnetron discharge configuration than that in the post-cathode configuration. The maximum absolute values of the discharge current obtained in the post-cathode and inverted magnetron discharge configurations were 0.111 and 0.375 A, respectively, at 200 G magnetic field.

3.2 *Discharge current–magnetic field characteristics*

Figures 5a and 5b show the discharge current (I)–magnetic field (B) characteristics of post-cathode and inverted magnetron discharge configurations, respectively. The operating pressure and the DC voltage were kept constant while the externally applied magnetic field was varied and the discharge current was observed. As shown in figure 5a, the discharge current increases with increasing magnetic field in the post-cathode magnetron discharge. However, in the case of inverted magnetron discharge, for the same operating conditions, the discharge current varied differently with increasing magnetic field. Here, the discharge current gradually increased with increasing magnetic field, attained a maximum value at a sufficiently higher magnetic field and got saturated (figure 5b). In the post-cathode magnetron, with the increasing magnetic field, electrons will get more confined and travel relatively longer paths in the discharge region thereby increasing the probability to participate in more ionisation collisions. This increased probability enhances the overall electron flux reaching the anode, thereby increasing the discharge

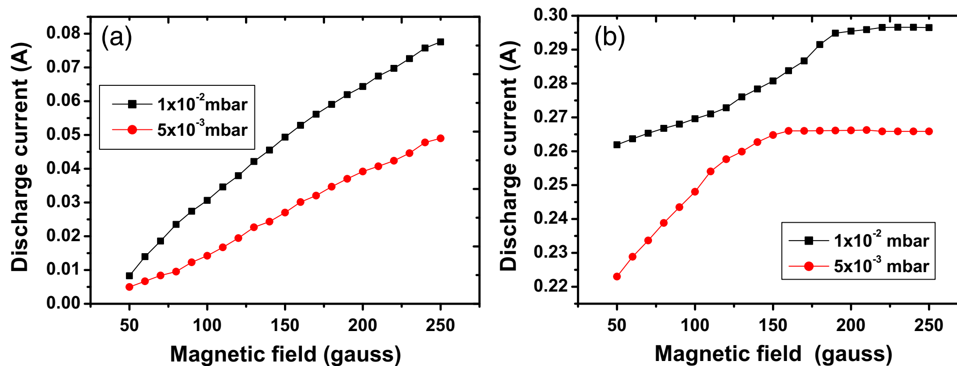

Figure 5. Discharge current–magnetic field characteristics of (**a**) post-cathode and (**b**) inverted configuration.

current. But in the case of inverted magnetron discharge, the *I–B* curve follows the same trend as it was in the post-cathode configuration up to a certain value of magnetic field and for the same reasons. However, as the magnetic field reaches a sufficiently high value, the discharge current reaches a maximum value and gets saturated. The reason for this is that at higher magnetic fields, the electron space charge gets accumulated near the anode resulting in a steep electric field gradient near the anode and less field near the cathode [14]. The cathode fall decreases due to reduction in mobility of electrons across the magnetic field. Hence, the probability of electrons escaping from the cathode decreases, limiting the discharge current. The discharge current is dependent upon the plasma formation near the anode and its expansion with magnetic field in the case of inverted discharge. The discharge current gets saturated at 0.26 A for $P = 5 \times 10^{-3}$ mbar, and at an increased value of 0.29 A for $P = 1 \times 10^{-2}$ mbar which is shown in figure 5b. In both magnetron discharges, at a given applied voltage and magnetic field, the absolute value of discharge current was observed to be more at higher operating pressures. The electrons experience more ionising collisions in the presence of magnetic field at higher operating pressures. This leads to an increase in the drift of electrons in radial direction, thereby increasing the discharge current.

3.3 *Plasma potential measurement*

Figure 6 shows the plasma potential profile from the anode to the cathode in both post-cathode and inverted magnetron configurations. The plasma potential was derived from the saturated floating potential obtained from emissive probe measurements. The plasma potential was measured with reference to the negative electrode, i.e. cathode. All the measurements were conducted at constant magnetic field $(B) = 100$ G, pressure $(P) = 5 \times 10^{-3}$ mbar and discharge voltage $(V) =$

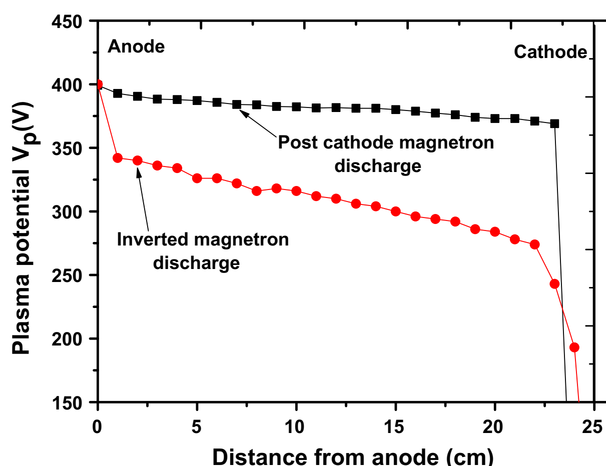

Figure 6. Plasma potential profile for both the configurations.

400 V. The radial profile of the plasma potential distribution in the post-cathode magnetron discharge shows potential gradient near the cathode, which is due to the presence of ion sheath and the potential is almost constant throughout the remaining discharge regions. However, in the case of inverted magnetron discharge, the radial plasma potential distribution has a different trend. Plasma potential is higher towards the anode, and it gradually decreases while moving away from the anode, and becomes less positive towards the cathode. The strong anode fall was also observed in the case of inverted configuration. In inverted magnetron discharge, the cathode area is larger than the anode area. The ion loss is more compared to the electron loss because ions remain less magnetised compared to electrons. The electron diffusion across the magnetic field decreases. The anode glow formation takes place near the anode due to strong anode fall. This anode glow is formed due to extra ionisation in front of the electron sheath and this glow is visible to the naked eye. This glow further expands

into the thick anode glow at higher magnetic field. In order to balance electron and ion flux leaving from the discharge, a potential is developed near the anode due to which electrons get accelerated and eventually lost to anode.

3.4 *Particle balance for electrons and ions*

The amount of ion loss from the plasma must be balanced by an equal amount of electron loss to maintain quasineutrality during the steady-state operation. The electron flux lost through the electron sheath is given by [21]

$$J_{\mathrm{e}} = \frac{n_{\mathrm{e}} e \alpha_{\mathrm{ee}}}{4}\sqrt{\frac{8T_{\mathrm{e}}}{\pi m_{\mathrm{e}}}}, \tag{1}$$

where α_{ee} is the transmission coefficient of electrons incident on electron sheath. As all the electrons incident on the electron sheath are lost, $\alpha_{\mathrm{ee}} = 1$. The transmission coefficient of ions incident on the electron sheath is neglected because the electron sheath potential drop is much greater than the ion temperature. Similarly, the ion flux lost through the Bohm sheath is given by

$$J_{\mathrm{i}} = n_{\mathrm{i}} e \alpha_{\mathrm{ii}}\sqrt{\frac{T_{\mathrm{e}}}{m_{\mathrm{e}}}}, \tag{2}$$

where α_{ii} is the transmission coefficient of ions incident on the ion sheath. Since the Bohm pre-sheath reduces the ion density at the sheath edge for the retarding potential barrier, $\alpha_{\mathrm{ee}} = 0.5$. The electron transmission coefficient incident on the ion sheath is neglected because the ion sheath potential drop is much higher than the electron temperature. Now multiplying eqs (1) and (2) with electron loss area and ion loss area, respectively, and then equating both for global particle balance in quasineutral plasma gives

$$\frac{A_{\mathrm{i}}}{A_{\mathrm{e}}} = \sqrt{\frac{2m_{\mathrm{i}}}{\pi m_{\mathrm{e}}}}, \tag{3}$$

where A_{i} and A_{e} are the areas for ion loss current and electron loss current, respectively. In the case of argon plasma, the right-hand side factor of eq. (3) comes as ∼215. Hence, if the ratio of ion loss area to the electron loss area is greater than ∼215, the electron sheath formation will takes place. In the case of post-cathode configuration, the area of electron collecting surface, i.e. anode, is much greater than that of the cathode. However, in the case of inverted magnetron, the physical area of the anode is small compared to the cathode. In addition, due to transverse magnetic field, the electron flux reaching the anode is reduced sufficiently resulting in the reduction of effective electron loss area. Hence, the plasma potential becomes more negative with respect to the anode to push the electrons to the anode through the electron sheath.

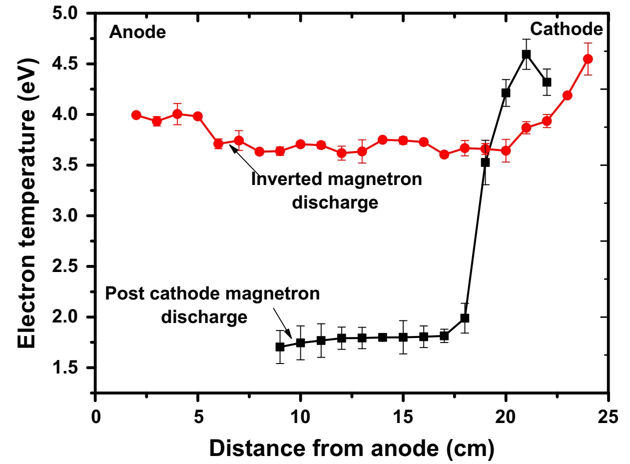

Figure 7. Electron temperature profile in both configurations.

3.5 *Electron temperature measurement*

The radial profiles of electron temperature in post-cathode and inverted magnetron discharges are shown in figure 7. The electron temperature was determined from the I–V characteristics of the double Langmuir probe. All measurements were conducted at the constant discharge voltage $(V) = 400$ V, pressure $(P) = 5 \times 10^{-3}$ mbar and magnetic field $(B) = 100$ G. As we can see in figure 7, in post-cathode magnetron discharge, the electron temperature is higher near the cathode, i.e. at the boundary of the cathode sheath. The electron temperature starts decreasing and becomes constant after some distance away from the cathode. The maximum was found to be at 3 cm away from the cathode with a value of 4.5 eV. However, in the inverted magnetron discharge, the radial electron temperature distribution was observed to be different. In this case, the electron temperature was found to be decreasing with the distance away from the cathode up to 4 cm and becomes constant after that in the intermediate region. However, near the anode region, a little rise in electron temperature was observed. In the case of post-cathode magnetron discharge, the electron temperature goes on decreasing radially away from the cathode because the electrons lose their energy in collisions and ionisation while travelling away from the cathode. In the inverted magnetron discharge, the same phenomenon was observed near the cathode. However, the observed rise in the electron temperature near the anode is due to the energy gain of electrons in the positive anode

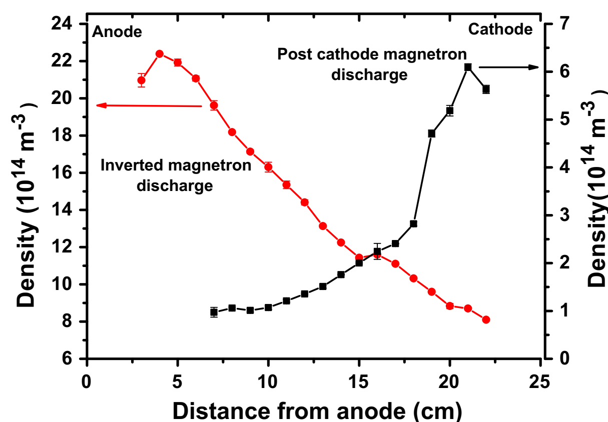

Figure 8. Plasma density profile for both configurations.

fall. The overall electron temperature in the inverted magnetron discharge is higher compared to that of the post-cathode magnetron discharge. This higher electron temperature can be due to the enhanced electric field (i.e. finite potential gradient) in the positive column region compared to the positive column of the post-cathode configuration (see figure 6). The electron temperature measurements could not be carried out near the anode in the case of post-cathode configuration, because the probe current signal was very less due to low-density plasma.

3.6 *Plasma density measurement*

The radial profile of plasma density for the post-cathode and inverted magnetron discharges are shown in figure 8. The experimental conditions such as discharge voltage, operating pressure and magnetic field were maintained the same as mentioned in the previous section. In the post-cathode magnetron discharge, the plasma density was high near the cathode and decreases with distance towards the anode. But, in inverted magnetron discharge, the plasma density was higher near the anode and decreases towards the cathode. Maximum plasma densities were observed 3–4 cm away from the inner electrode in both magnetron discharges. This is because in both magnetron discharges the electrons get trapped in the area close to and surrounding the inner electrode so that most of the ionisation and excitation occurs in that area. The absolute value of plasma density in the post-cathode magnetron discharge is, however, lower when compared with that in the inverted magnetron discharge under comparable experimental conditions. The radial plasma density profiles in both magnetron discharges are almost opposite to each other.

3.7 *Thin film deposition*

In order to understand the effect of the type of discharge on the crystallinity and surface morphology, copper thin films were deposited using both the configurations. Copper was used as the target material, i.e. cathode, and silicon wafer was used as the substrate over which the films were deposited. In the post-cathode configuration, copper rod of 4 mm diameter and 70 mm length was used as the cathode while an SS tube of 100 mm inner diameter and 140 mm length was used as the anode. In the inverted configuration, a copper tube of 100 mm inner diameter was used as the cathode and an SS rod of 4 mm diameter was used as the anode. The ratio of the surface area of the cathode to that of the anode was maintained around 50, similar to the one that was maintained during plasma characterisation studies discussed previously. Silicon wafers, over which coating would be deposited and characterised, were placed on the anode surface. The deposition parameters such as DC power (i.e. 100 W), argon pressure ($P = 5\times10^{-2}$ mbar), deposition time (30 min) and externally applied magnetic field (100 G) were kept constant in both the configurations. The crystal structure of the deposited thin film was studied using the XRD analysis, while the thickness and surface morphology of the thin film were studied using SEM. Figure 9 shows the SEM images of pure copper film deposited on the silicon wafer. In the case of post-cathode configuration, it is observed that the surface of the film shows little porosity and consists of compact spherical nanostructures of approximately 50–80 nm in size as shown in figure 9a. However, in inverted configuration, the films deposited show porosity or voids between nanostructures. The larger grain structure consisting of agglomerates of small crystallites can be observed in the micrograph (figure 9b). The size of these structures is large compared to the size of the nanostructures of the film deposited using the post-cathode discharge. The plasma formation due to the anode fall near the anode in the case of inverted configuration has influenced the film properties. The increase in localised temperature due to plasma particle bombardment helps in increasing the size of the nanostructures. The adatom surface diffusion and grain growth are dependent upon substrate temperature [22]. In the case of inverted configuration, the temperature near the anode increases due to extra plasma formation which modifies the film properties. In addition, the large oblique component of the sputtered flux in the case of inverted configuration affects the film growth. Figure 10 shows the cross-sectional images of thin film indicating the structure and thickness of the deposited film. This figure clearly shows that the film growth is columnar in nature and thickness is around 1700 nm for

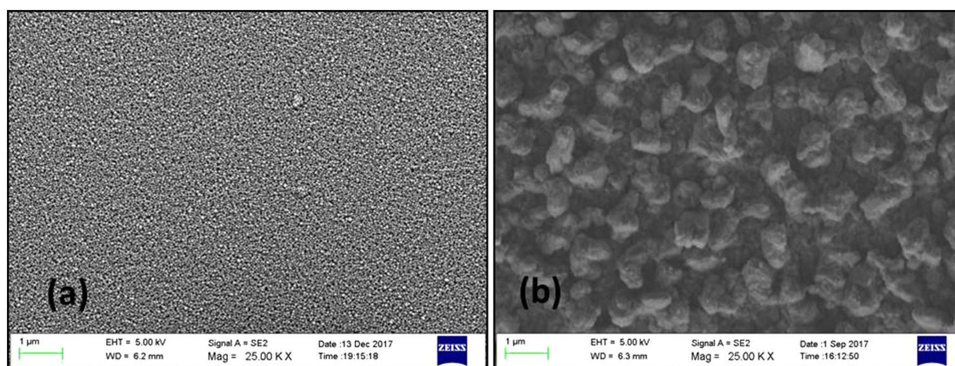

Figure 9. Surface morphology of copper thin film deposited by using (**a**) post-cathode and (**b**) inverted configurations.

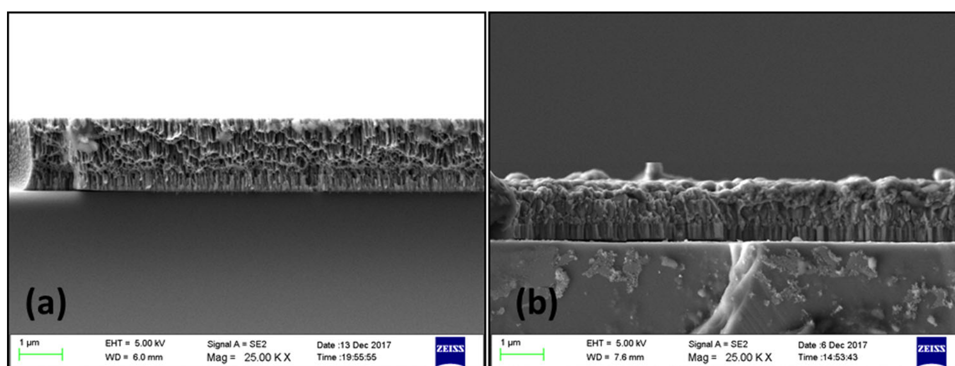

Figure 10. Cross-sectional images of copper thin film deposited by using (**a**) post-cathode and (**b**) inverted configurations.

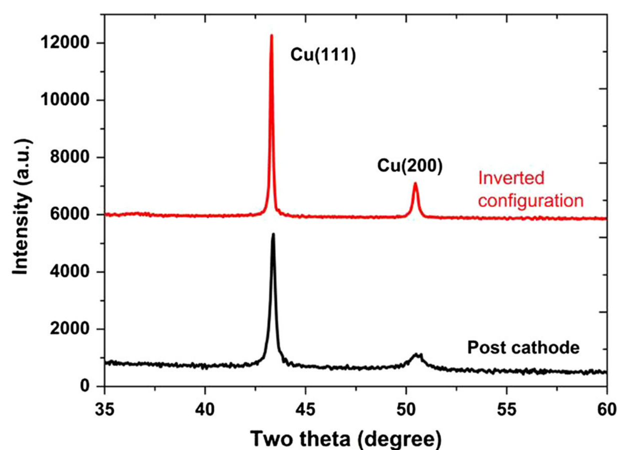

Figure 11. XRD peaks of the copper film.

post-cathode and 1500 nm for inverted configurations. Figure 11 shows XRD patterns of thin films deposited in both configurations. XRD patterns of both the films are similar. The analysis of these XRD patterns indicates that peaks arising at $2\theta \sim 43.5^\circ$ and $2\theta \sim 50.8^\circ$ are reflections from (1 1 1) and (2 0 0) planes of cubic copper, respectively. However, the peaks were observed to be broad in the case of post-cathode configuration, indicating smaller crystallite size.

4. Conclusion

The discharge characteristics of post-cathode and inverted cylindrical magnetron discharges were studied. The current–voltage characteristics show magnetron mode of operation for both discharges. It was observed that the discharge current increases with magnetic field in the case of post-cathode configuration while it saturates at higher magnetic field in the case of inverted magnetron. The plasma potential was almost constant in the positive column of the post-cathode configuration while it decreases from anode to cathode for inverted magnetron. A potential fall of 20–25 V was observed near the anode in inverted magnetron configuration, which was absent in the case of post-cathode discharge. The maximum plasma density and electron temperature were found to be near the inner electrode in both the discharges. The copper thin films deposited using both the discharges show different surface morphology, though the XRD studies show similar peaks. The size of the copper crystallites is larger in inverted configuration, due to the bombardment by high-density plasma near the anode. Hence, the film properties can be tailored using the appropriate electrode configuration, i.e. post-cathode or inverted in cylindrical magnetron discharges. For example, the large grain size and voided structure of

copper deposited using the inverted configuration suggests the possibility of improving the solar absorbance of such films containing copper element. Further, as the resistivity of the copper film with larger grain size is less, the inverted configuration can be used for the copper film applications in interconnection wires of integrated electronic circuits.

References

[1] J A Thornton, *J. Vac. Sci. Technol.* **15**, 171 (1978)
[2] P J Kelly and R D Arnell, *Vacuum* **56(3)**, 159 (2000)
[3] J Hon, *J. Phys. D* **42(4)**, 043001 (2009)
[4] A A Atta, M M El-Nahass, K M Elsabawy, M M Abd El-Raheem, A M Hassanien, A Alhuthali, A Badawi and A Merazga, *Pramana – J. Phys.* **87**: 72 (2016)
[5] D Hoffman, *Thin Solid Films* **96**, 217 (1982)
[6] T A Van der Straaten, N F Cramer, I S Falconer and B W James, *J. Phys. D* **31**, 177 (1998)
[7] T A Van der Straaten, N F Cramer, I S Falconer and B W James, *J. Phys. D* **31**, 191 (1998)
[8] P Kudrna and E Passoth, *Contrib. Plasma Phys.* **37**, 417 (1997)
[9] G Y Yeom, J A Thornton and M J Kushner, *J. Appl. Phys.* **65**, 3816 (1989)
[10] E Passoth, P Kudrna, C Csambal, J F Behnke, M Tichy and V Helbig, *J. Phys. D* **30**, 1763 (1997)
[11] A R Pal, J Chutia and H Bailung, *Phys. Plasmas* **11**, 4719 (2004)
[12] J A Thornton, *Thin Solid Films* **54**, 23 (1978)
[13] J A Thornton, *J. Vac. Sci. Technol.* **17**, 380 (1980)
[14] R Rane, M Bandyopadhyay, M Ranjan and S Mukherjee, *Phys. Plasmas* **23**, 013514 (2016)
[15] W D Gill and E Kay, *Rev. Sci. Instrum.* **36(3)**, 277 (1965)
[16] Y Golubovskii, I A Porokhova, V P Sushkov, M Holik, P Kudrna and M Tichy, *Plasma Sources Sci. Technol.* **15**, 228 (2006)
[17] O V Vozniy, D Duday, I Luciu and T Wirtz, *Plasma Sources Sci. Technol.* **23**, 045011 (2014)
[18] D A Duarte, M Massi, A S da Silva Sobrinho, H S Maciel, K Grigorova and L C Fontana, *Eur. Phys. J. Appl. Phys.* **49**, 13107 (2010)
[19] A Todoran, M Mantel, A Bes, C Vachey and A Lacoste, *Plasma Sources Sci. Technol.* **23**, 065039 (2014)
[20] M A Makowski and G A Emmert, *Rev. Sci. Instrum.* **54(7)**, 830 (1983)
[21] B Longmier, S Baalrud and N Hershkowitz, *Rev. Sci. Instrum.* **77**, 113504 (2006)
[22] S Craig and G Harding, *J. Vac. Sci. Tecnol.* **19(2)**, 205 (1981)